Final Draft
of the original manuscript:

Nöchel, U.; Behl, M.; Balk, M.; Lendlein, A.:
Thermally-Induced Triple-Shape Hydrogels: Soft Materials Enabling Complex Movements.
In: ACS Applied Materials and Interfaces. Vol. 8 (2016) 41, 28068 – 28076.
First published online by ACS: 27.09.2016

http://dx.doi.org/10.1021/acsami.6b09581

Thermally-Induced Triple-Shape Hydrogels – Soft Materials Enabling Complex Movements

Ulrich Nöchel[a], Marc Behl[a,b], Maria Balk[a,b] and Andreas Lendlein[a,b,*]

[a] Institute of Biomaterial Science and Berlin-Brandenburg Center for Regenerative Therapies (BCRT), Helmholtz-Zentrum Geesthacht, Kantstr. 55, 14513 Teltow (Germany)
[b] Tianjin University - Helmholtz-Zentrum Geesthacht, Joint Laboratory for Biomaterials and Regenerative Medicine, Kantstr. 55, 14513 Teltow (Germany)
E-mail: andreas.lendlein@hzg.de

Keywords: shape-memory, triple-shape, hydrogels, stimuli-sensitive materials, X-ray scattering

Abstract

Shape-memory hydrogels enable directed movements of a specimen in response to temperature, whereby crystallizable switching segments incorporated as side chains resulted in constant degrees of swelling during the shape-memory cycle. Here we report about hydrogels exhibiting a thermally-induced triple-shape effect which allow complex movements of soft materials with two almost independent shape changes. Potential applications for those soft triple-shape materials are two-step self-unfolding devices or temperature-sensitive hydrogel actuators, e.g. smart valves for flow rate control in aqueous media. Series of hydrogels with two different hydrophobic crystallizable switching segments were prepared. The degrees of swelling of the triple-shape hydrogels were not affected for different shapes or temperatures, avoiding in this way interferences on the shape shifts. During the two-step programming procedure two distinct shapes can be implemented as reflected by shape fixity ratios of generally > 50%. Structural analysis of the switching domains during the triple-shape cycle by means of X-ray scattering indicate that longer side chains gain lower orientation after deformation and that shorter side chains orient perpendicular to the hydrophilic main chain. Furthermore, it is observed that increased orientation of the switching domains is not a key requirement for adequate shape fixity and recovery ratios of the triple-shape effect in hydrogels, thus longer side chains can be utilized as switching segments in other shape-memory hydrogels.

Introduction

Hydrogels with shape-changing or shape-memory capability[1-3] provide on one hand soft tissue-like mechanical properties and have the ability to store large amounts of water, mimicking biological environments,[4-5] on the other hand these stimuli-sensitive hydrogels are capable to respond to a stimulus like temperature, changes in pH,[6-14] or a variation of the concentration of ions.[15-17] More recently, supramolecular approaches focused on self-healing applications.[16, 18-19] Often the response to the stimulus is accompanied by a volume change caused by swelling and de-swelling mechanisms resulting in non-directed movements.[20-21] Hydrogels exhibiting a directed movement by means of a thermally-induced shape-memory effect (SME) were reported for polymer networks of crosslinked poly(acrylic acid) with stearyl acrylate side chains and were denoted as shape-memory hydrogels.[22-24] In these systems a deformation of a permanent shape into a temporary shape could be fixed by crystallized switching segments, and once the melting temperature of the switching segments was exceeded the permanent shape was recovered. The switching temperature (T_{sw}) of the hydrogel was correlated to a thermal transition temperature (T_{trans}) of switching domains provided by stearyl side groups. Dual-shape hydrogels with stearyl or shorter alkyl side chains and hydrophilic polypeptide side chains have been described.[25-26] More recently, a double-network hydrogel enabled the combination of shape-memory and shape-changing effects.[27] However, for some specific applications of soft materials where complex directed movements are required, e.g. intelligent valves to enable the control of the flow rate by the actuation process of the hydrogel, more than one temporary shape might be required. Thus the material should be capable to perform two distinct directed movements, resulting in this way in an *in-situ* actuation on demand.[28] This kind of effect, known as triple-shape effect (TSE), was realized for the first time in copolymer networks consisting of poly(ε-caprolactone) and poly(ethylene glycol) segments named CLEG or of poly(cyclohexyl methacrylate) and poly(ε-caprolactone) segments named MACL,[29] followed by other copolymer- and blend-based triple-shape polymers.[30-34] Thermally-induced triple-shape or even

multi-shape effects have been intensively investigated as they enable successive directed movements of a specimen in a single shape recovery cycle upon heating, extending in this way the potential field of application.[35-36] Compared to hydrogels with SME, hydrogels with TSE could extent the field of applications for materials, which mimic the biological environment and permit two subsequent directed movements on demand. In this context, hydrogels based on acrylonitrile were explored as triple-shape polymers, which acted sensitive to the presence of zinc ion species and their concentration by dynamic association and dissociation.[37] Also the combination of the presence of calcium ions and changes in pH value were reported as stimuli for a TSE in hydrogels obtained by the polymerization of acrylamide in the presence of phenylboronic acid-grafted alginate and poly(vinyl alcohol).[38] Recently, polyacrylamide based hydrogels with dansyl-aggregates and azo-cyclodextrins acting as switches were reported to initiate two distinct movements by the subsequent utilization of changes in pH value and application of light.[39] For these types of triple-shape hydrogels challenging recovery processes utilizing different stimuli were required. Therefore, an important advantage of a TSE in hydrogels would be the realization of complex directed movements in aqueous media of different composition solely thermally controlled by the solidification/melting of the switching segments. In this way just heat as an easily applicable stimulus would trigger the two recovery processes. Hereby the field of potential applications of triple-shape hydrogels would be tremendously broadened, as the actuation would become independent of the chemical composition of the swelling agent and no direct contact would be necessary between the sample and the source of stimulus as it is required in the case of ions.

Nonetheless, some challenges for realizing a thermally-induced triple-shape effect in hydrogels need to be resolved. Compared to dry bulk polymer networks the presence of water and the volume increase by swelling influence the structure of the polymer network, which can result in different material requirements for realizing a TSE. The requirement for realizing a TSE is sufficient elasticity of the material to perform two successive deformations during the

programming procedure. In hydrogels, i.e. polymer networks in the swollen state, the molecular chains are already in a less coiled, extended form, which might reduce the maximum possible elongation of the specimen. The formation of temporary physical netpoints by crystallizable switching segments can also influence the degree of swelling and in this way may counteract to the SME. One possibility to realize a constant volume upon formation of physical netpoints is the utilization of switching segments incorporated as side chains. Shape-memory hydrogels with oligo(ω-pentadecalactone) (oPDL)[40] or oligotetrahydrofuran (oTHF)[41] side chains exhibited relatively constant degrees of swelling above and below the melting temperature of the switching segments. We have selected semi-crystalline switching segments for realizing a TSE in hydrogels as glass transitions are affected or suppressed by bound water.[42-43] In addition the degree of crystallinity or crystallization kinetics of the switching segment could be influenced or reduced in the presence of water. In order to enable crystallization in the swollen state, hydrophobic switching segments were selected.

We hypothesized that two types of crystallizable switching segments, forming crystallizable domains having T_ms separated by at least 20 K, could be co-polymerized with a hydrophilic monomer, forming the network's backbone when using telechelic precursors. These mono-functionalized oligomers would be grafted on a hydrophilic main chain and a polymer network could be created by copolymerizing a crosslinking agent in a one-step reaction. Various types of oligomers were considered as side chains regarding the targeted difference of 20 K in T_{trans}: oligo(ε-caprolactone) (oCL) (T_m between 35 °C and 60 °C as function of M_n), oPDL (T_m between 70 °C and 90 °C), and oTHF (T_m between 15 °C and 30 °C). In addition, stearyl side chains provided by stearyl acrylate were selected as an example for grafted chains of low molecular weight. N-Vinylpyrrolidone (NVP) was selected to create the backbone of the swollen polymer networks as polymers of NVP exhibit high wettability.[44-45] A low molecular weight and hydrophilic crosslinker, oligo(ethylene glycol) dimethacrylate ($oEG_{200}DMA$), was selected to avoid its crystallization and to support the swelling in water. The resulting hydrogels

were characterized in terms of swelling behavior, thermal and mechanical properties, and the capability of a TSE was explored. Furthermore, the nanostructure of the semi-crystalline switching segments was studied by X-ray scattering techniques in order to gain insights to the mechanism of the TSE in hydrogels regarding the crystallization behavior of the switching segments such as crystal orientation as function of oligomer type and chain length and crystal sizes, which determine the TSE properties.

Experimental Section

Synthesis. Telechelic oligomers were prepared and functionalized with 2-isocyanoethyl-methacrylate (IEMA) according to a described procedure.[40] Polymer networks were prepared by mixing the telechelic precursors, NVP, oEG_{200}-DMA and AIBN (1.5 mol% related to all vinyl, acrylate, and methacrylate groups) with a concentration of 70 wt% reactants in 1,4-dioxane. The mixture was poured between glass plates equipped with a 2 mm Teflon® spacer, which were kept at 75 °C for 24 h and subsequently extracted with 1,4-dioxane.

Characterization. Tensile tests and shape-memory experiments were performed using standard test specimen (ISO 527-2/1BB) on a Zwick 2.5 (Zwick, Ulm, Germany), equipped with a 20 N load cell at a deformation rate of 10 $mm \cdot min^{-1}$. The tensile clamps were submerged in a 10 L distilled water tank, whose temperature was controlled by a Lauda ECO (Lauda, Lauda-Königshofen, Germany). The cyclic thermomechanical tests consisted of six cycles, in which the first one was the preconditioning cycle. In the following the permanent shape is denoted as shape C, the first temporary shape as shape B, and the second temporary shape as shape A. Each cycle consisted of a triple-shape creation procedure (TSCP) and a recovery module. In both modules a heating and cooling rate of 1 $K \cdot min^{-1}$ was used. During the TSCP the sample was heated to T_{high}, equilibrated for 3 min, deformed to a programming strain for shape B $\varepsilon_{B,load}$ (typically 50%) and cooled to T_{mid} under constant strain. Afterwards the stress was released after 20 min resulting in ε_B. Then the sample was deformed to a programming

strain for shape A $\varepsilon_{A,load}$ (typically 75%), cooled to T_{low} under constant strain, and T_{low} was kept for 20 min. After releasing the stress, ε_A was obtained. Temporary shape B and permanent shape C were recovered by heating from T_{low} to T_{high}. The triple-shape properties are computed for the individual transitions, i.e. shape C→B and B→A. For each transition the shape fixity ratio R_f and the shape recovery ratio R_r were calculated with Equation 1 and Equation 2:

$$R_{f,B\to A} = \frac{\varepsilon_A - \varepsilon_B}{\varepsilon_{A,load} - \varepsilon_B} \cdot 100 \qquad (1)$$

$$R_{r,A\to B} = \frac{\varepsilon_A - \varepsilon_{B,rec}}{\varepsilon_A - \varepsilon_B} \cdot 100 \qquad (2)$$

The WAXS investigations were performed on a Bruker D8 Discover with a two-dimensional detector (HI-Star) from Bruker AXS (Karlsruhe, Germany). The X-ray generator producing copper K-α radiation with a wavelength of 0.154 nm was operated at a voltage of 40 kV and a current of 40 mA. A graphite monochromator and a pinhole collimator with an opening of 0.8 mm defined the optical and geometrical properties of the beam. A custom-build setup with a stretching device, a heating gun and a cooled nitrogen gas stream allowed *in-situ* X-ray diffraction measurements to be performed at different stages during the programming cycle of the samples. The diffraction images were collected at a sample to detector distance of 15 cm. Isotropic two-dimensional diffraction images were integrated to obtain plots with intensity versus scattering angle and the crystallinity index was determined using the software TOPAS® from Bruker.

SAXS was performed on a Bruker Nanostar, operating 40 kV and 35 mA on a copper anode. Point focussed X-rays were monochromated and parallelized by Montel-optics and collimated by a 750/400/1000 µm 3-pinhole combination, thus a 400 µm beam having a wavelength of 0.154 nm was obtained. The distance sample to detector was 1070 mm calibrated with Silver behenate standard. Exposure time was 3 h on a Vantec-2000 detector (2048 x 2048 pixel, 68 µm pixel size).

Results and discussions

Synthesis of the hydrogels. Oligomers with one telechelic hydroxy function were prepared by ring-opening polymerization of the corresponding momomers using 1-hexanol as initiator. The polymerization of oligoesters was catalyzed by dibutyl tin oxide and the polymerization of oligoethers by trifluoromethanesulfonic anhydride (Tf_2O). The obtained hydroxy-terminated telechelic oligomers were subsequently modified with IEMA resulting in methacrylated end groups. The resulting oligomers had a number average molecular weight M_n of 1900 g·mol^{-1} for oCL-IEMA, 2500 g·mol^{-1} for oPDL-IEMA, and 6700 g·mol^{-1} for oTHF-IEMA as determined by GPC, exhibiting a T_m of 48, 89, and 31 °C, respectively.

Series of polymer networks with two switching segments were prepared in 1,4-dioxane from NVP, oEG_{200}-DMA crosslinker and the methacrylated switching segment by free radical polymerization using AIBN as initiator (the structural formula of the polymer network is visualized in Figure 1d). Hydrogels could be obtained, after extraction with 1,4-dioxane and subsequent reconditioning of the obtained polymer networks with H_2O. The hydrogels were denoted as *X*(*a*)*Y*(*b*) in which *X* and *Y* represent the switching segments (abbreviating oPDL as P, oCL as C, oTHF as T, and stearyl acrylate as S) and *a* and *b* denote the weight contents in wt% of the IEMA-functionalized switching segment in the starting reaction mixture related to the overall dry mass of precursors. Thus a sample denoted as P(10)C(20) consist of 10 wt% oPDL-IEMA, 20 wt% oCL-IEMA, and 70 wt% NVP.

The following criteria were used for the selection of types and weight contents of side chain segments for the hydrogels with two switching segments: (a) switching domains must exhibit distinct and separated T_ms, (b) the hydrogels should provide a volumetric degree of swelling in water higher than 200%. On the one hand the incorporation of hydrophobic components would reduce the water uptake of hydrogels, the content of oPDL, oCL, oTHF, and stearly acrylate

should be low. On the other hand, a sufficient amount of crystalline domains is required to enable the fixation of the temporary shape. Therefore, oPDL-IEMA in a weight content of 10 wt% was selected to be co-polymerized with different ratios of the second switching segment, varying from 10 to 40 wt% for oCL-IEMA and 10 to 30 wt% for stearyl acrylate. In contrast to oCL and stearyl acrylate, the oligomer oTHF exhibits a lower hydrophobic character, whereby the crystallization in an aqueous environment might be slightly suppressed. Hence, the content of oTHF-IEMA as second switching segment was varied between 20 and 50 wt%. In addition, two series with 20 or 5 wt% of oPDL-IEMA and 10 to 30 wt% of stearyl acrylate were synthesized to investigate the influence of the oPDL-IEMA weight content on the behavior of the second switching segment (e.g. thermal properties, shape fixity and recovery ratios). The molecular architecture of hydrogels with two types of side chains of different oligomer chain lengths is presented in Figure 1b and c and the resulting properties are resumed in Table 1.

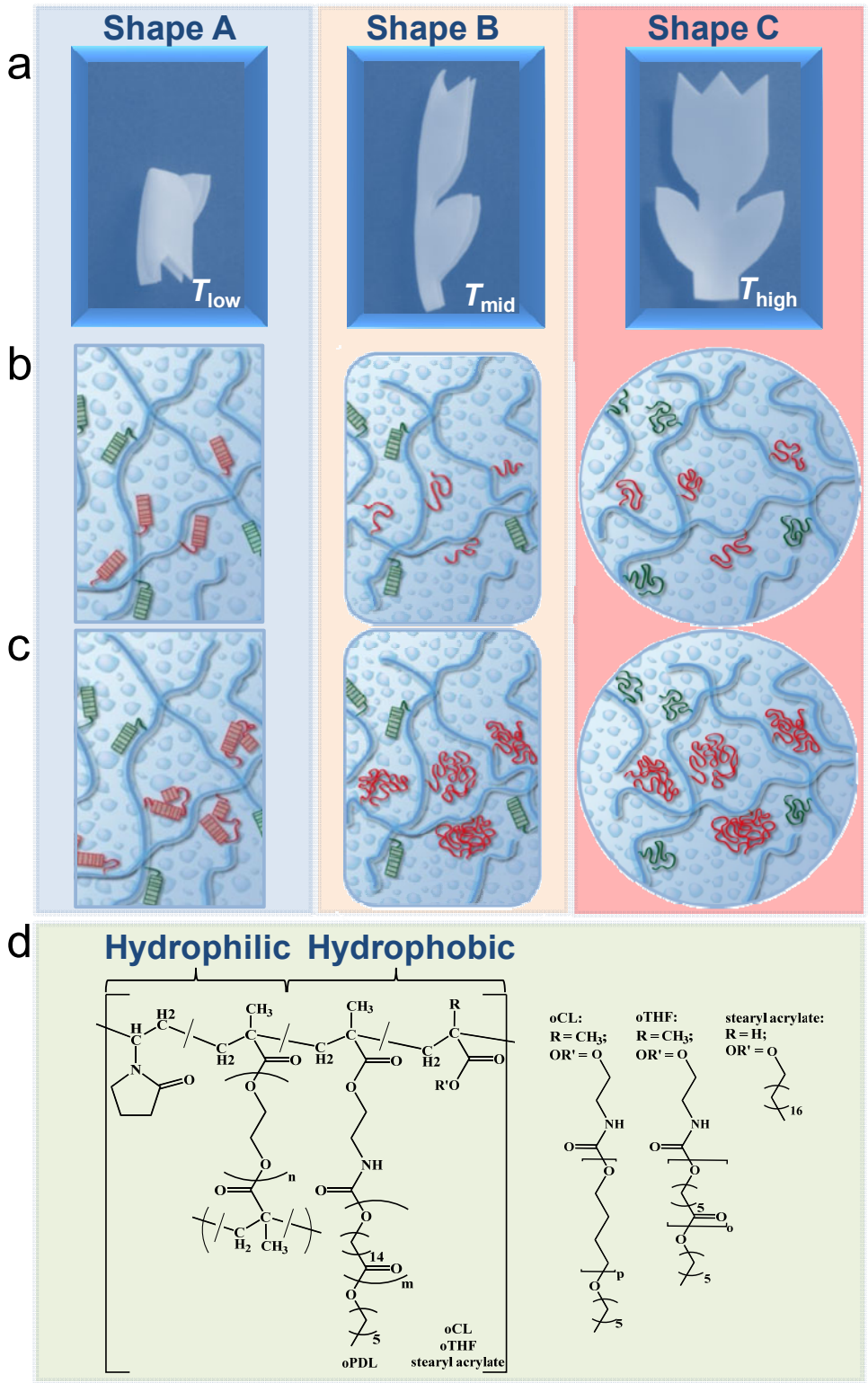

Figure 1. Recovery process of a triple-shape hydrogel. (**a**) Series of photographs representing the triple-shape effect of a P(10)S(20) hydrogel on a demonstrator of a tulip in a temperature-controlled water bath. Shape A: T_{low} = 10 °C, shape B: T_{mid} = 60 °C, shape C: T_{high} = 90 °C. (**b**) and (**c**) Schemes of molecular structures of the switching segments of the second temporary shape A at T_{low}, the first temporary shape B at T_{mid}, and the permanent shape C at T_{high} with different oligomer chain lengths exhibiting different crystalline orientations. (**d**) Chemical structure of the polymer network.

Swelling experiments of the permanent shape. In order to detect a possible influence of the temperature on the equilibrium swelling of the systems, the volumetric degree of swelling in water Q was determined for all series from equilibrium swollen hydrogels at the relevant temperatures, i.e., at T_{low} = 10 °C, T_{mid} = 60 °C, and T_{high} = 90 °C. First the gel content Gc was determined as the resulting polymer networks were extracted with 1,4-dioxane (Table 1). The high yield of the crosslinking reaction was reflected by Gc > 89%. On extracted samples the swelling experiments were performed. A relatively high degree of swelling in water was obtained for all P(10)Y(b) series, exhibiting a minimum Q ~ 250% for the systems P(10)C(40) and P(10)S(30). P(20)S(30) had Q ~ 200% (Table 1). The P(10)T(b) series presented an increasing Q with increasing weight content of the oTHF side chain due to its slightly hydrophilic character, as oTHF has the highest number of oxygen atoms of all Y-segments per repeating unit. Figure 2a visualizes this behavior for hydrogels having P(10)Y(b) composition. Furthermore, Q was found to be independent of the temperature, remaining almost constant at T_{low}, T_{mid}, and T_{high} for the permanent shape C (Figure 2a and Table 1), which was attributed to a similar hydrophobicity of the switching segments in the semi-crystalline and the amorphous state. In contrast, hydrogels with a low content of oPDL as presented for the series of P(05)S(b) exhibited a relatively low decrease of Q when the temperature was increased from T_{low} to T_{mid}, which correlates to the transition of stearyl acrylate as non-oligomeric aliphatic side chain from the semi-crystalline to the amorphous state. Therefore, oligomeric side chains prevent an additional uptake of water when the temperature is increased, which could be attributed to the formation of entanglements resulting in large hydrophobic areas, which are present in the semi-crystalline and in the amorphous state. In contrast, short side chains have less tendency to create physical netpoints by entanglements and could therefore not prevent an additional swelling in water when the temperature is increased. From these findings, we deduced that two oligomeric switching segments incorporated as side chains are beneficial for enabling directed movements by almost avoiding swelling effects at different temperatures.

Thermal properties. The compliance of two separated melting transitions in the hydrogels with two hydrophobic switching segments was explored by thermal analysis on equilibrium swollen specimens. The thermal properties of the series of hydrogels were determined by differential scanning calorimetry whereby two well defined T_ms (Table 1 and Figure 2b) were detected. The P(10)C(b) hydrogels exhibited a $T_{m,oPDL}$ almost constant around 85 °C over the composition range of oCL and $T_{m,oCL}$ increased from 40 to 45 °C with increasing oCL weight content. The P(a)T(b) systems exhibited similar behavior, with $T_{m,oPDL}$ ~ 85 °C and an increase of $T_{m,oTHF}$ from 23 to 30 °C. Use of stearyl acrylate side chains in the P(a)S(b) hydrogels resulted in a decreased $T_{m,oPDL}$ (80 to 73 °C) with decreasing oPDL content, which was attributed to a steric hindrance of the oPDL chains with the randomly distributed stearyl side chains. Because of the short chain length of the stearyl group (C18), it is more often inserted in the backbone of the polymer network and therefore hindered the oPDL crystallization slightly. This interference suggests the advantage for switching segments of high molecular weight when aiming for constant T_ms within series of hydrogels with two switching segments. Nonetheless, all systems presented two separated melting transitions, which could enable the fixation of two temporary shapes utilizing crystalline reversible physical crosslinks.

To investigate the kinetics of thermal transitions, which define the time period required to enable the fixation of the shape, the time periods necessary for the melting and crystallization of the switching segment were determined by DSC measurements with heating and cooling rates in the range from 1 $K \cdot min^{-1}$ to 20 $K \cdot min^{-1}$. At a rate of 1 $K \cdot min^{-1}$, all thermal transition of switching segments in hydrogels were completed within 20 min (Figure S1), which was the time period between the beginning and the end of the corresponding melting and crystallization thermal transitions. The increase of the rate drastically decreased the time period, in which both thermal transitions occurred to 2 min indicating in this way the dependence of heating and

cooling rates on the transition between a semi-crystalline and an amorphous state of the integrated switching segments.

Table 1. Swelling experiments and thermal properties of the hydrogels with two switching segments

Sample ID	*Gc* [a]	*Q* [b]	*Q* [b]	*Q* [b]	T_m(P) [c]	T_m(Y) [c]	ΔH_m(P) [c]	ΔH_m(Y) [c]
	[%]	10 °C, [%]	60 °C, [%]	90 °C, [%]	[°C]	[°C]	[J·g^{-1}]	[J·g^{-1}]
P(20)S(10)	97 ± 2	250 ± 50	230 ± 20	250 ± 40	81 ± 2	23 ± 2	15.4	1.3
P(20)S(20)	95 ± 1	290 ± 60	260 ± 40	290 ± 30	79 ± 2	33 ± 2	19.1	5.4
P(20)S(30)	97 ± 4	210 ± 70	190 ± 40	190 ± 40	77 ± 2	37 ± 2	13.1	7.1
P(10)S(10)	96 ± 1	460 ± 30	420 ± 10	440 ± 70	75 ± 2	33 ± 2	5.2	1.5
P(10)S(20)	98 ± 1	330 ± 10	310 ± 10	310 ± 30	76 ± 2	40 ± 2	5.4	6.5
P(10)S(30)	97 ± 1	280 ± 20	290 ± 20	260 ± 50	76 ± 2	42 ± 2	total	14.7
P(05)S(10)	93 ± 2	480 ± 50	390 ± 40	370 ± 60	78 ± 2	35 ± 2	2.9	3.1
P(05)S(20)	97 ± 2	470 ± 70	390 ± 20	390 ± 10	75 ± 2	41 ± 2	1.2	4.3
P(05)S(30)	98 ± 1	370 ± 60	280 ± 10	280 ± 10	73 ± 2	43 ± 2	0.9	5.6
P(10)C(10)	97 ± 3	550 ± 50	600 ± 50	570 ± 30	88 ± 2	n.d.	3.7	n.d.
P(10)C(20)	94 ± 6	430 ± 70	310 ± 40	320 ± 40	86 ± 2	40 ± 2	3.6	3.0
P(10)C(30)	91 ± 9	290 ± 10	290 ± 10	300 ± 70	87 ± 2	42 ± 2	5.7	6.9
P(10)C(40)	93 ± 6	260 ± 10	270 ± 30	250 ± 10	87 ± 2	45 ± 2	4.0	11.8
P(10)T(20)	97 ± 1	430 ± 10	430 ± 40	480 ± 50	87 ± 2	23 ± 2	5.4	1.8
P(10)T(30)	91 ± 4	570 ± 70	520 ± 50	520 ± 30	88 ± 2	24 ± 2	total	2.5
P(10)T(40)	92 ± 1	620 ± 50	610 ± 60	560 ± 80	87 ± 2	30 ± 2	1.5	1.2
P(10)T(50)	89 ± 3	560 ± 30	600 ± 50	550 ± 30	87 ± 2	30 ± 2	2.9	3.1

[a] Determined by gravimetric relation of raw and extracted dry polymer networks. [b] Determined by gravimetric relation of dry and swollen polymer networks and the densities of water and polymer network. [c] Determined from the second DSC heating run. [d] n.d., not detected

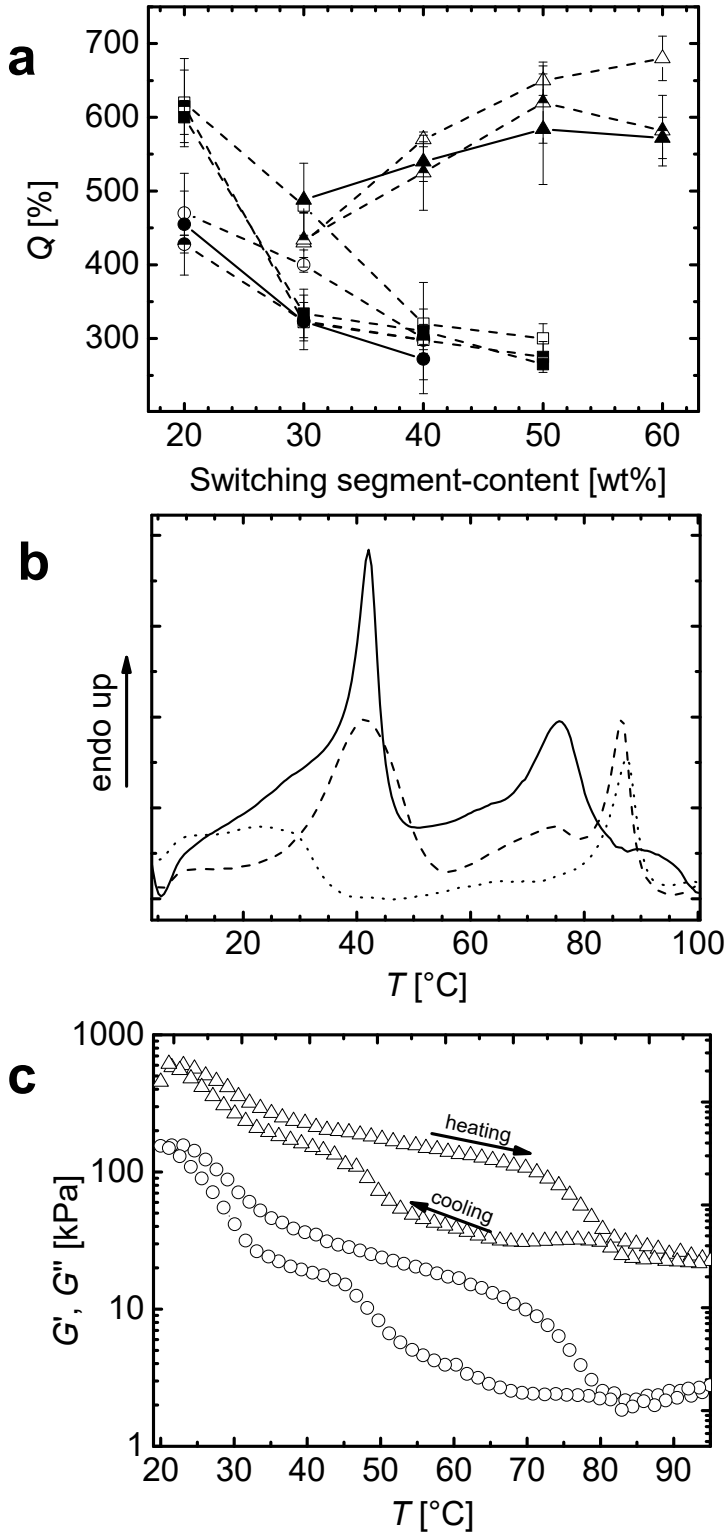

Figure 2. (a) Volumetric degree of swelling in water of the hydrogels consisting of two switching segments. Triangle up represents P(10)T(b), circles P(10)S(b), and squares P(10)C(b) hydrogels (empty symbols T_{low}, half-filled symbols T_{mid}, and filled symbols T_{high}). **(b)** Second DSC heating curves of the swollen hydrogels P(10)S(30) (continuous line), P(10)C(30) (discontinuous line) and P(10)T(30) (dotted line), exhibiting sharp and distinct melting endotherms. (**c)** Exemplary temperature sweep by rheometry of P(10)S(20) during a heating-cooling cycle with shear storage (triangles) and shear loss (circles) moduli.

Mechanical properties. The elasticity of the hydrogels is primarily related to the length of the polymer chain segments between two chemical crosslinks, whereby longer chain segments will result in an increased elasticity of the polymer network. When hydrophilic main chain segments are utilized and the polymer network is swollen, the entropy of the system is reduced caused by the stretching of the formerly randomly coiled polymer chains, resulting in a decrease of the elongation at break. As the incorporation of hydrophobic side chains extends the polymer chain segment length by one repeating unit, the contribution to the elasticity and swelling would be marginal. Nonetheless, side chains can exhibit entanglements and hydrophobic associations, which will result in additional physical netpoints and could slightly reduce the degree of swelling and the overall elasticity of the hydrogel. Another aspect is the state of aggregation of the switching segment. Crystallizable hydrophobic switching segments can influence the mechanical properties of the hydrogels by the level of organization, i.e. amorphous or semi-crystalline. In summary, the composition, i.e. the weight content of hydrophobic side chain and the type will determine the mechanical properties of the designed hydrogels.

For determining these influences, the mechanical properties were determined at T_{low}, T_{mid}, and T_{high} (Table 2) by means of rheometric heating-cooling runs as shown in Figure 2c. The shear storage and shear loss moduli (G' and G'') presented two transitions with increasing T related to $T_{trans,1}$ and $T_{trans,2}$ of the switching segments and reached a plateau at T_{high}, which reflected the chemical netpoints of the hydrogels. G' was always higher than G'' and demonstrated the elastic character over the whole T-range. At T_{low}, P(10)S(b) and P(10)C(b) hydrogels presented similar shear moduli $G = \sqrt{G'^2 - G''^2}$, ranging from 200 to 500 kPa, whereas the P(10)T(b) hydrogels exhibited Gs around 50 kPa, which was related to the soft mechanical properties of the oTHF side chains. Here, the longer oTHF side chains presented an advantage when aiming for very soft mechanical properties as hydrogels with the lowest shear moduli were obtained.

An increasing weight content of oPDL caused an increase of G in the order P(05)S(b) < P(10)S(b) < P(20)S(b). In these series, G was found to be relatively constant

(within the margin of error) and almost independent of the weight content of the Y-segments (exemplary shown in Figure S2 with P(a)S(b) hydrogels). Potentially contributions of both types of physical netpoints, that are, the crystalline fractions and the entanglements in the amorphous phase, resulted into relative constant shear moduli. At T_{mid}, the increasing oPDL weight content increased *G* from 50 kPa for P(05)Y(b), 100 kPa for P(10)Y(b) and 200 to 400 kPa for P(20)Y(b) series as expected from the amount of crystallized fraction (only oPDL). Hydrogels of the P(10)S(b) series had slightly higher shear moduli *G* (~120 kPa) than P(10)C(b) series (30 to 100 kPa). P(10)T(b) hydrogels exhibited *G*s from 13 to 36 kPa. *G* was found to be independent within the margin of error. These findings may be attributed to the length of the side chains. Shorter side chains at equal weight fractions were more often present in the backbone of the polymer network and reduced its mobility, which resulted in an increased shear modulus. This result became more evident at T_{high}, when both switching segments were amorphous and *G*s were higher in the P(10)S(b) systems (20 to 40 kPa) as compared to the P(10)C(b) series (10 to 30 kPa) and were lowest in the P(10)T(b) series (constant around 6 kPa). Here an increase of the modulus within a series was observed for P(10)S(b), P(05)S(b), and P(10)C(b) hydrogels. As only few entanglements were expected from the stearyl side chains, the reduction of the backbone mobility seemed to have a strong influence on the shear modulus. Again the longer side chains presented some advantage over low molecular weight chains resulting in softer materials with more uniform mechanical properties.

Table 2. Triple-shape and thermo-mechanical properties of hydrogels with two switching segments.

Sample ID	R_f(C→B) [a]	R_f(B→A) [a]	R_f(A→B) [a]	R_r(A→C) [a]	R_r(B→C) [a]	$T_{trans,1}$ [b]	$T_{trans,2}$ [b]	$G(T_{low})$ [b]	$G(T_{mid})$ [b]	$G(T_{high})$ [b]
	[%]	[%]	[%]	[%]	[%]	[°C]	[°C]	[kPa]	[kPa]	[kPa]
P(20)S(10)	91 ± 1	77 ± 2	69 ± 3	89 ± 1	97 ± 3	28 ± 2	81 ± 2	220 ± 40	160 ± 10	48 ± 6
P(20)S(20)	95 ± 1	90 ± 1	70 ± 4	90 ± 2	90 ± 2	29 ± 2	80 ± 2	1240 ± 120	400 ± 30	27 ± 1
P(20)S(30)	84 ± 4	90 ± 4	74 ± 2	93 ± 3	94 ± 7	34 ± 2	78 ± 2	940 ± 70	190 ± 10	29 ± 1
P(10)S(10)	64 ± 8	83 ± 7	89 ± 1	88 ± 6	91 ± 7	32 ± 2	79 ± 2	360 ± 190	120 ± 50	23 ± 1
P(10)S(20)	59 ± 5	95 ± 1	91 ± 4	97 ± 1	95 ± 5	37 ± 2	80 ± 2	450 ± 50	120 ± 20	28 ± 3
P(10)S(30)	51 ± 4	96 ± 2	90 ± 3	96 ± 2	94 ± 6	42 ± 2	78 ± 2	190 ± 10	105 ± 4	42 ± 1
P(05)S(10)	60 ± 4	86 ± 9	87 ± 9	89 ± 5	95 ± 6	37 ± 2	80 ± 2	250 ± 140	35 ± 5	10 ± 1
P(05)S(20)	43 ± 2	95 ± 2	95 ± 2	96 ± 1	97 ± 3	40 ± 2	76 ± 2	320 ± 70	39 ± 4	14 ± 3
P(05)S(30)	37 ± 6	97 ± 2	93 ± 2	84 ± 3	96 ± 4	41 ± 2	76 ± 2	300 ± 1	53 ± 6	34 ± 1
P(10)C(10)	79 ± 2	81 ± 6	66 ± 4	85 ± 4	92 ± 8	36 ± 2	80 ± 2	220 ± 120	60 ± 20	12 ± 1
P(10)C(20)	72 ± 2	80 ± 5	62 ± 8	83 ± 2	89 ± 5	42 ± 2	81 ± 2	150 ± 3	32 ± 1	19 ± 1
P(10)C(30)	58 ± 4	85 ± 5	68 ± 9	87 ± 3	93 ± 4	45 ± 2	88 ± 2	220 ± 5	50 ± 3	22 ± 3
P(10)C(40)	53 ± 6	89 ± 2	74 ± 3	89 ± 3	91 ± 9	44 ± 2	78 ± 2	540 ± 70	100 ± 10	27 ± 1
P(10)T(20)	84 ± 2	69 ± 4	47 ± 4	76 ± 4	85 ± 4	26 ± 2	80 ± 2	51 ± 1	36 ± 1	6 ± 1
P(10)T(30)	70 ± 2	89 ± 6	60 ± 9	84 ± 3	78 ± 6	26 ± 2	88 ± 2	42 ± 2	19 ± 1	6 ± 1
P(10)T(40)	50 ± 4	81 ± 8	62 ± 9	77 ± 9	80 ± 8	28 ± 2	88 ± 2	30 ± 1	13 ± 2	5 ± 1
P(10)T(50)	37 ± 2	80 ± 5	49 ± 4	82 ± 6	93 ± 5	30 ± 2	88 ± 2	63 ± 1	25 ± 4	7 ± 1

[a] Determined by cyclic thermomechanical tensile tests as an average of five cycles, whereby the applied deformation from shape C to shape B was 50% and from shape B to shape A was 75% (additional 25%) strain. [b] Determined by rheometric heating scans at 1 $K \cdot min^{-1}$.

Determination of triple-shape properties. The required elasticity of the hydrogels for programming two temporary shapes was explored by tensile tests until failure with a strain rate of 5 $mm \cdot min^{-1}$, which exhibited an elongation at break $\varepsilon_b > 50\%$ at T_{high} and $\varepsilon_b > 75\%$ at T_{mid} for all materials, and by this set the maximum deformation for the investigations of a potential triple-shape effect of the hydrogels. The triple-shape capability of hydrogels with two crystallizable domains was explored in cyclic thermomechanical experiments. A TSCP was applied on the sample to implement the triple-shape capability. During TSCP the specimen was heated to T_{high} and deformed to $\varepsilon_{B,load} = 50\%$. When the material was cooled under external stress to T_{mid} ($T_{trans,1} < T_{mid} < T_{trans,2}$), physical crosslinks were formed by crystallization of one

switching segment. Shape B was obtained after release of the external stress. Shape A was created subsequently by deformation of shape B to $\varepsilon_{A,load}$ = 75% at T_{mid} and cooled to T_{low} (T_{low} < $T_{trans,1}$ < $T_{trans,2}$) under external stress, thus crystallizing the second switching segment. The release of the external stress resulted in shape A. Reheating to T_{mid} recovered shape B and subsequent heating to T_{high} resulted in shape C.

The shape fixity (R_f) and recovery (R_r) ratios are listed in Table 2. The shape fixity of the first temporary shape R_f(C→B) was dominated by the oPDL content as the recrystallization of this oligomeric side chain prevented the recovery to the permanent shape C. For this reason R_f(C→B) increased from 40 to 90% when the oPDL content was increased from P(05)S(b) to P(20)S(b). Furthermore, R_f(C→B) decreased with increasing weight content of the second switching segment, which does not contribute to the shape fixation. While the weight contents of the second switching domains (i.e. the Y segments) became higher than 20 wt% the probability of encountering adjacent oPDL side chains is lowered and thus R_f(C→B) was reduced. The shape fixity ratios after programming the second temporary shape R_f(B→A) are listed in Table 2. R_f(B→A) increased with increasing Y-segment content up to 97% for P(X)S(Y) series, 89% for P(10)C(Y) series, and 89% for the P(10)T(Y) hydrogels, whereby the increased shape fixity was attributed to the higher wt% of the crystallizable Y-segments as more physical netpoints could be created after cooling to T_{low}.

The R_rs from the second temporary shape A to the first temporary shape B (R_r(A→B)) remained relatively constant within a series, being 60 to 70% for P(10)C(b) series, 50 to 60% for P(10)T(b) series, and 90% for P(10)S(b) systems. The recovery of the permanent shape (R_r(B→C)) was only governed by the entropic elasticity of the amorphous polymer network as both crystallizable switching domains were molten and R_rs(B→C) > 90% were obtained. The overall recovery (R_r(A→C)) represented the contribution of both previous transitions (a photo series of the process is shown in Figure S3). The TSE on a P(10)S(20) hydrogel is demonstrated as fotoseries in Figure 1, where the molecular structure in dependence of the oligomer chain

length of the three shapes is presented. Here a permanent shape was a tulip (shape C) which was folded to shape B and finally to the temporary shape A. In the photo series the recovery process is observed, where shapes B and C were subsequently re-obtained upon heating the water bath from T_{low} to T_{high}. The sketch of the molecular structure (Figure 1b and c) shows the conformations of the hydrogel in shape A with both switching segments in the semi-crystalline state, recovered shape B by melting one switching segment, and recovered shape C with both switching segments in the amorphous state.

The application potential of triple-shape hydrogels becomes apparent in a demonstration device for a valve capable of controlling the flow rate of water upon increase of temperature (see Supporting Video S1). Here, the actuator of one single triple-shape hydrogel sample was equipped with two orifices; one was programmed at 90 °C and the other at 60 °C. The sample was inserted at the end of a translucent tube, which was continuously flushed with water, whereby the temperature of the water was raised from 25 °C to 90 °C. At 25 °C both orifices were open resulting in the highest flow rate of water. When the temperature reached 45 °C, first the orifice programmed at 60 °C closed resulting in a noticeable reduction of the flow rate. When the temperature was further raised to 80 °C the second orifice closed, which stopped the flow. In this way the smart valve could control three flow rates upon an increase of temperature.

In order to investigate the swelling behavior of the hydrogels during the triple-shape cycle, Q was determined for the temporary shapes B and A at T_{mid} and T_{low} respectively (Supplementary Table S1). Q of the temporary shapes was comparable to Q of the permanent shape within the margin of error, which was attributed to a relative constant volume resulting from the side chain character of the hydrophobic switching segments. When a switching segment was amorphous, in the molten state, its hydrophobicity still repealed water and no additional swelling took place. The network architecture of the crosslinked pNVP hydrophilic main chain resulted in constant chain length between netpoints and enabled a relative constant swelling over the temperature range and the three shapes of the hydrogels. In this way, it could be confirmed that only directed

complex movements of the specimens and no swelling effects contributed to the TSE of the hydrogels with crystallizable hydrophobic switching segments incorporated as side chains.

Evolution of the semi-crystalline nanostructure during the TSE. In order to get insight into the molecular mechanism of the fixation and recovery processes, structural investigations were performed by meaning of SAXS and WAXS techniques on the permanent shape C and the temporary shapes B and A during the triple-shape cycle of the hydrogels.

The analysis of the WAXS curves of the non-deformed, isotropic materials (shape C) at room temperature revealed crystal unit cell dimensions, calculated as d-spacing from the peak positions, according to literature.[46-49] The average lateral crystal sizes l_c perpendicular to the evaluable lattice planes (i.e. 110-planes for oPDL and oCL and 020- and 202-planes for oTHF) were obtained via the Scherrer equation[50]. Size l_c was found to be independent of the mass fraction in the polymer network for P(10)C(b) (both ~16 nm) systems. For P(a)S(b) series, l_c as determined from the (110)-reflection was contributed by oPDL and stearyl crystals, and decreased with increasing stearyl and decreasing oPDL content with values from 17 nm to 8 nm. This was related to a smaller l_c of stearyl (~8 nm) compared to oPDL and oCL. In the P(10)T(b) hydrogels, the crystal size of oPDL remained constant (~16 nm) whereas the crystal size of oTHF increased with increasing weight fractions (~10 to 18 nm). We attributed the increased oTHF crystal size to the longer chain length of oTHF and increased wt% of oTHF could lead to extended crystallization. Switching segments of shorter chain lengths had a wider distribution in the network's backbone and could only crystallize to a limited size. Thus oPDL, oCL, and stearyl presented relative constant l_c.

Figure 3-I exhibit the azimuthal profiles of crystalline reflections once the TSCP was completed. The green line is the (020) reflection of oTHF crystals, red line is a superposition of (110) reflection from oPDL and stearyl lateral chain packing, and blue line is a superposition of (110) reflections from oPDL and oCL. Generally with a higher degree of crystal orientation a more

pronounced peak profile is observed. Thus the orientation increased in order P(10)T(Y) < P(10)C(Y) < P(10)S(Y), which was related to the molecular weight of the switching segment. Side chains of low molecular weight (e.g. stearyl) aligned easily perpendicular to the deformed backbone. The perpendicular alignment could be concluded from the position of the peak maxima on the meridian. Nonetheless oTHF side chains, which had the highest molecular weight, did almost exhibit no orientation after TSCP but were still capable of fixing a second temporary shape (see R_f in Table 2). To elucidate the behavior of the switching segments in terms of crystallization and melting further X-ray experiments were conducted. Figure 3-II shows the scattering patterns obtained during a triple-shape cycle, exemplary shown for P(10)S(20). In this way, patterns of Fig. 3-IIa (WAXS) and Fig. 3-IIe (SAXS) were taken from the permanent shape C. Debye-Scherrer rings in the WAXS pattern indicated an isotropic, non-oriented nanostructure, with crystalline (110) and (220) reflections. The (110) reflection was a superposition of oPDL and stearyl reflections. The SAXS pattern also exhibited a ring-like reflection (isotropic), which was related to contributions of the (001) signals of stearyl chains and contributions of the (001) reflection of the oPDL crystals (along the molecular axis). When the specimen was heated to T_{high} both WAXS (Fig. 3-IIb) and SAXS (Fig. 3-IIf) patterns did not show discrete scattering or reflections as both oPDL and stearyl were in the amorphous (molten) state. Only the WAXS pattern had a broad signal arising from water scattering and the amorphous halo. After deformation at T_{high} to $\varepsilon_{B,load}$ = 50% the patterns did not change. When the sample was cooled to T_{mid} the oPDL switching segment could crystallize and fix the temporary shape B (see recorded patterns of Fig. 3-IIc and Fig. 3-IIg). Two weak reflections in the WAXS pattern were observed, being the (110) stronger, which had a slight intensity distribution along the ring and with maxima on the meridian (drawing direction), indicating that the oPDL crystals were somehow anisotropic and would have the molecular axis along the equator (perpendicular to drawing). This finding was also observed in the SAXS pattern, where scattering maxima are found on the equator, which were attributed to the (001) reflection of the

oPDL, i.e., the signal along the molecular axis. Nevertheless, the degree of orientation was not high as the ring-like character was still visible. When the sample was deformed to $\varepsilon_{A,load}$ = 75% at T_{mid} and subsequently cooled to T_{low} the stearyl was able to crystallize and fix the temporary shape A (see recorded patterns of Fig. 3-IId and Fig. 3-IIh). The crystalline WAXS (110) reflection presented increased intensity with a clear maxima towards the meridian. This was related to the contribution of crystalline stearyl inter-chain signals, where the stearyl molecular axis was perpendicular to the meridian (drawing direction) and thus to the NVP-backbone of the polymer network. This observation is confirmed by the SAXS pattern, where the scattering maxima is more pronounced and clearly focused on the equator. We resume that oPDL and stearyl side chains showed a tendency to orient perpendicular to the drawing direction, which was related to the short chain length as presented in Figure 1b. This orientation behavior of switching segments with low molecular weight was in good agreement to non-swollen polymer networks as reported for side chains of poly(ethylene glycol) in CLEG polymer networks.[51] Nevertheless, it can be noticed that a thermally induced triple-shape effect in hydrogels did not require strong crystalline orientation as the oTHF switching segments with a higher oligomer chain length (Figure 1c) were able to fix a temporary shape properly (R_f up to 89%). High R_f was enabled by an almost non-oriented crystallization resulting from low molecular alignment after the deformation step, which was attributed to the higher mobility of the long side chain as compared to short side chains. Thus, long side chains, i.e. switching segments of high molecular weight, can be utilized for triple-shape hydrogels and in this way permit the tailoring of the switching temperature by selecting an adequate molecular weight.

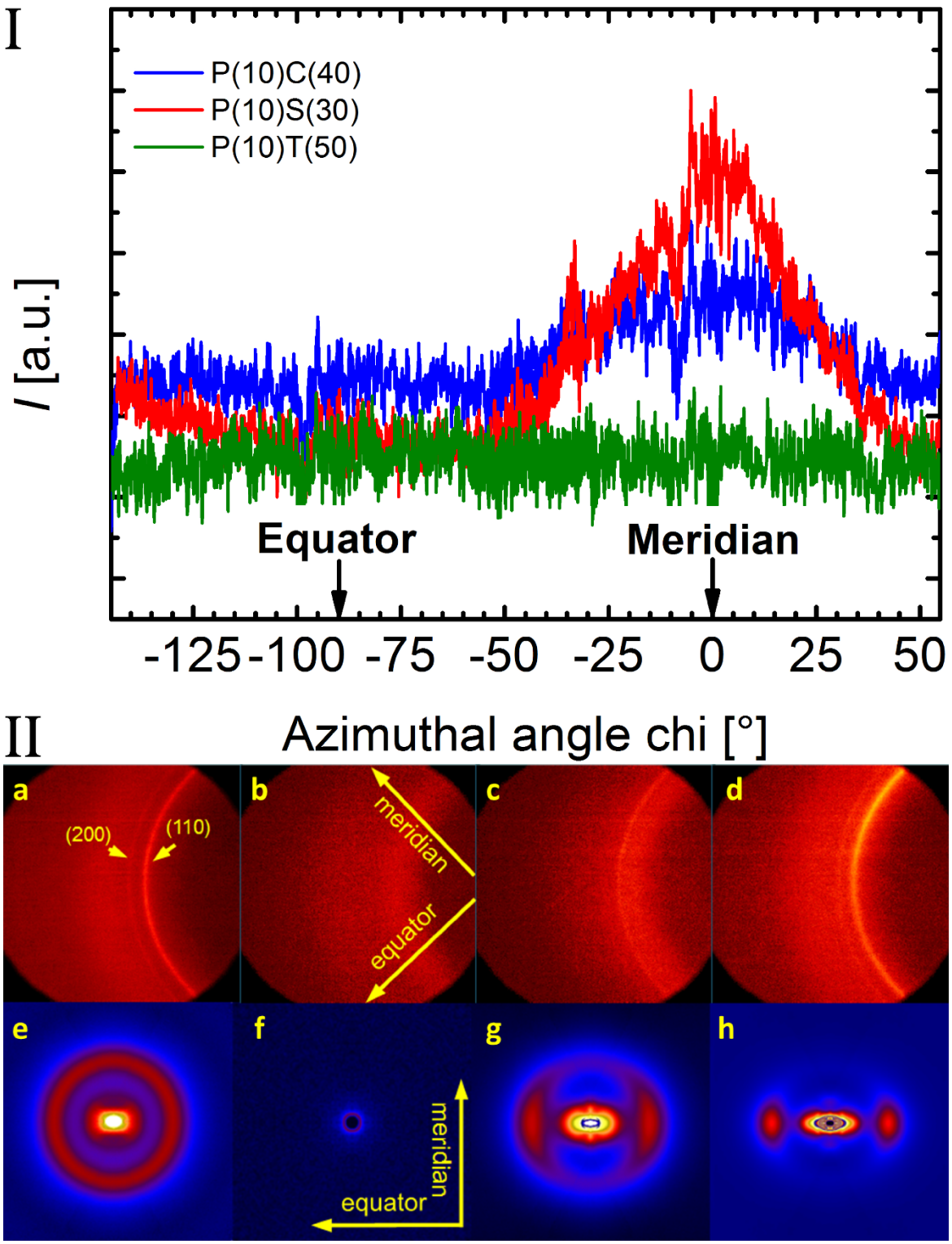

Figure 3. (I) Azimuthal Profiles of crystalline reflections of hydrogels in the second temporary shape A obtained from WAXS. Green line is the (020) reflection of oTHF crystals, red line is a superposition of (110) reflection from oPDL and Stearyl lateral chain packing, and blue line is a superposition of (110) reflections from oPDL and oCL. The higher the orientation the more pronounced the peak profile with maxima on the meridian (indicated). **(II)** Two dimensional WAXS (a to d) and SAXS (e to h) patterns recorded for shape C (a and e) at T_{low}, the amorphous state at T_{high} (b and f), the first temporary shape B (c and g) at T_{mid}, and second temporary shape A (d and h) at T_{low}. Directions of meridian (drawing direction) and equator are indicated.

Conclusion

The present work describes the design of hydrogels capable of a thermally-induced triple-shape effect by combining a hydrophilic network with two types of hydrophobic crystallizable switching segments, which were incorporated as side chains. An influence of the temperature on the swelling of the permanent shape was not detected, which enabled the implementation of directed movements, regardless shape-changing effects caused by different swelling. The systems provided soft mechanical properties in the kPa range, which mainly depended on the type of the second switching segment, whereby longer oTHF side chains resulted in advantageously soft mechanical properties. The materials were found to be sufficiently elastic for two deformations required for programming a triple-shape effect and had sufficiently separated melting transitions. It was observed that longer side chains had the advantage of not affecting the melting transitions of the second switching segment. Shape fixity ratios of the temporary shapes were found to depend on the weight content of the switching domains. Increasing wt% of the related switching segment increased the fixity of the related temporary shape but decreased the fixity of the other temporary shape. By appropriate adjustment of their ratio, R_f(C→B) and R_f(B→A) could be optimized for P(20)S(20) (both $R_fs \geq 90\%$), P(10)C(10) ($R_fs = 80\%$), and P(10)T(30) ($R_fs = 70$ and 90%). R_r(A→C) was found to be higher than 90%. Swelling experiments during the TSE indicated no influence on the different shapes, and directed movements of the specimens could be concluded. Analysis of the semi-crystalline nanostructure revealed that shorter side chains tend to orient perpendicular to the drawing direction, and longer side chains result in almost isotropic crystallization after deformation. Thus, orientation of the switching segment is not a requirement for a TSE in hydrogels. This might enable the utilization of novel types of switching segments in shape memory hydrogels, which could extend the field of application for soft materials capable of complex movements in aqueous media utilizing a single and simple trigger for the shape recovery processes. In this

way, three flow rates could be controlled upon an increase of temperature in a device equipped with a triple-shape valve.

Supporting Information

Figure S1. Determination of kinetics of thermal transitions with the example of P(10)S(10) by variation of heating and cooling rates.

Figure S2. Mechanical properties of hydrogels as function of oPDL wt% and content of stearyl acrylate.

Figure S3. Demonstration of programming and recovery process of a triple-shape hydrogel by elongation as deformation type.

Table S1. Volumetric degrees of swelling of the first temporary shape B at T_{mid} and the second temporary shape A at T_{low}.

Video S1. Smart valve based on thermally-induced triple-shape hydrogels capable to control the flow rate.

Acknowledgements

This work has been financially supported by the Helmholtz Association through programme oriented funding and the Tianjin University-Helmholtz-Zentrum Geesthacht, Joint Laboratory for Biomaterials and Regenerative Medicine, which is financed by the German Federal Ministry of Education and Research (BMBF, Grant No. 0315496) and the Chinese Ministry of Science and Technology (MOST, 2008DFA51170).

References:

(1) Slaughter, B. V.; Khurshid, S. S.; Fisher, O. Z.; Khademhosseini, A.; Peppas, N. A. Hydrogels in Regenerative Medicine. *Adv. Mater.* **2009**, *21*, 3307-3329.
(2) Jagur-Grodzinski, J. Polymeric Gels and Hydrogels for Biomedical and Pharmaceutical Applications. *Polymer. Adv. Techn.* **2010**, *21*, 27-47.
(3) Madsen, J.; Armes, S. P. (Meth)acrylic Stimulus-Responsive Block Copolymer Hydrogels. *Soft Matter* **2012**, *8*, 592-605.
(4) Lee, K. Y.; Mooney, D. J. Hydrogels for Tissue Engineering. *Chem. Rev.* **2001**, *101*, 1869-1880.

(5) Peppas, N. A.; Hilt, J. Z.; Khademhosseini, A.; Langer, R. Hydrogels in Biology and Medicine: From Molecular Principles to Bionanotechnology. *Adv. Mater.* **2006**, *18*, 1345-1360.
(6) Song, J. J.; Chang, H. H.; Naguib, H. E. Biocompatible Shape Memory Polymer Actuators with High Force Capabilities. *Eur. Polym. J.* **2015**, *67*, 186-198.
(7) Huynh, C. T.; Nguyen, Q. V.; Kang, S. W.; Lee, D. S. Synthesis and Characterization of Poly(amino urea urethane)-Based Block Copolymer and its Potential Application as Injectable pH/Temperature-Sensitive Hydrogel for Protein Carrier. *Polymer* **2012**, *53*, 4069-4075.
(8) Hu, X.; Kang, H.; Li, Y.; Li, M.; Wang, R.; Xu, R.; Qiao, H.; Zhang, L. Direct Copolycondensation of Biobased Elastomers Based on Lactic Acid with Tunable and Versatile Properties. *Polym. Chem.* **2015**, *6*, 8112-8123.
(9) Li, X.; Fan, D.; Ma, X.; Zhu, C.; Luo, Y.; Liu, B.; Chen, L. A Novel Injectable pH/Temperature Sensitive CS-HLC/beta-GP Hydrogel: The Gelation Mechanism and its Properties. *Soft Materials* **2014**, *12*, 1-11.
(10) Oh, Y. J.; In, I.; Park, S. Y. Temperature-Sensitive Hydrogel Prepared by Graft Polymerization of N-isopropylacrylamide onto Macroradical Pluronic. *J. Ind. Eng. Chem. (Amsterdam, Neth.)* **2012**, *18*, 321-324.
(11) Seol, D.; Magnetta, M. J.; Ramakrishnan, P. S.; Kurriger, G. L.; Choe, H.; Jang, K.; Martin, J. A.; Lim, T.-H. Biocompatibility and Preclinical Feasibility Tests of a Temperature-Sensitive Hydrogel for the Purpose of Surgical Wound Pain Control and Cartilage Repair. *J. Biomed. Mater. Res., Part B* **2013**, *101*, 1508-1515.
(12) Xu, X.; Song, J.; Wang, K.; Gu, Y.; Luo, F.; Tang, X.; Xie, P.; Qian, Z. Synthesis and Characterization of pH and Temperature Sensitive Hydrogel Based on Poly(N-isopropylacrylamide), Poly(epsilon-caprolactone), Methylacrylic Acid, and Methoxyl Poly(ethylene glycol). *Macromol. Res.* **2013**, *21*, 870-877.
(13) Gumel, A. M.; Annuar, M. S. M. Poly-3-hydroxyalkanoates-co-polyethylene Glycol Methacrylate Copolymers for pH Responsive and Shape Memory Hydrogel. *J. Appl. Polym. Sci.***2014**, *131*, DOI: 10.1002/app.41149.
(14) Hu, Y.; Lu, C.-H.; Guo, W.; Aleman-Garcia, M. A.; Ren, J.; Willner, I. A Shape Memory Acrylamide/DNA Hydrogel Exhibiting Switchable Dual pH-Responsiveness. *Adv. Funct. Mater.* **2015**, *25*, 6867-6874.
(15) Meng, H.; Zheng, J.; Wen, X.; Cai, Z.; Zhang, J.; Chen, T. pH- and Sugar-Induced Shape Memory Hydrogel Based on Reversible Phenylboronic Acid-Diol Ester Bonds. *Macromol. Rapid Comm.* **2015**, *36*, 533-537.
(16) Miyamae, K.; Nakahata, M.; Takashima, Y.; Harada, A. Self-Healing, Expansion-Contraction, and Shape-Memory Properties of a Preorganized Supramolecular Hydrogel through Host-Guest Interactions. *Angew. Chem. Int. Ed.* **2015**, *54*, 8984-8987.
(17) Nan, W.; Wang, W.; Gao, H.; Liu, W. Fabrication of a Shape Memory Hydrogel Based on Imidazole-Zinc Ion Coordination for Potential Cell-Encapsulating Tubular Scaffold Application. *Soft Matter* **2013**, *9*, 132-137.
(18) Chen, L.; Chen, H.; Yao, X.; Ma, X.; Tian, H. A Hybrid Supramolecular Polymeric Hydrogel with Rapid Self-Healing Property. *Chem. - Asian J.* **2015**, *10*, 2352-2355.
(19) Kakuta, T.; Takashima, Y.; Nakahata, M.; Otsubo, M.; Yamaguchi, H.; Harada, A. Preorganized Hydrogel: Self-Healing Properties of Supramolecular Hydrogels Formed by Polymerization of HostGuest-Monomers that Contain Cyclodextrins and Hydrophobic Guest Groups. *Adv. Mater.* **2013**, *25*, 2849-2853.
(20) Akintewe, O. O.; DuPont, S. J.; Elineni, K. K.; Cross, M. C.; Toomey, R. G.; Gallant, N. D. Shape-Changing Hydrogel Surfaces Trigger Rapid Release of Patterned Tissue Modules. *Acta Biomater.* **2015**, *11*, 96-103.

(21) Kim, S. J.; Kim, H. I. I.; Park, S. J.; Kim, S. I. Shape Change Characteristics of Polymer Hydrogel Based on Polyacrylic Acid/Poly(vinyl sulfonic acid) in Electric Fields. *Sens. Actuators, A* **2004**, *115*, 146-150.
(22) Mitsumata, T.; Gong, J. P.; Osada, Y. Shape Memory Functions and Motility of Amphiphilic Polymer Gels. *Polym. Adv. Tech.* **2001**, *12*, 136-150.
(23) Osada, Y.; Matsuda, A. Shape-Memory in Hydrogels. *Nature* **1995**, *376*, 219-219.
(24) Matsuda, A.; Sato, J.; Yasunaga, H.; Osada, Y. Order-Disorder Transition of a Hydrogel Containing an N-Alkyl Acrylate. *Macromolecules* **1994**, *27*, 7695-7698.
(25) Inomata, K.; Terahama, T.; Sekoguchi, R.; Ito, T.; Sugimoto, H.; Nakanishi, E. Shape Memory Properties of Polypeptide Hydrogels Having Hydrophobic Alkyl Side Chains. *Polymer* **2012**, *53*, 3281-3286.
(26) Kabir, M. H.; Hazama, T.; Watanabe, Y.; Gong, J.; Murase, K.; Sunada, T.; Furukawa, H. Smart Hydrogel with Shape Memory for Biomedical Applications. *J. Taiwan Inst. Chem. Eng.* **2014**, *45*, 3134-3138.
(27) Zhang, J. L.; Huang, W. M.; Gao, G.; Fu, J.; Zhou, Y.; Salvekar, A. V.; Venkatraman, S. S.; Wong, Y. S.; Tay, K. H.; Birch, W. R. Shape Memory/Change Effect in a Double Network Nanocomposite Tough Hydrogel. *Eur. Polym. J.* **2014**, *58*, 41-51.
(28) Zhao, Q.; Behl, M.; Lendlein, A. Shape-Memory Polymers with Multiple Transitions: Complex Actively Moving Polymers. *Soft Matter* **2013**, *9*, 1744-1755.
(29) Bellin, I.; Kelch, S.; Langer, R.; Lendlein, A. Polymeric Triple-Shape Materials. *PNAS* **2006**, *103*, 18043-18047.
(30) Zotzmann, J.; Behl, M.; Feng, Y.; Lendlein, A. Copolymer Networks Based on Poly(omega-pentadecalactone) and Poly(epsilon-caprolactone) Segments as a Versatile Triple-Shape Polymer System. *Adv. Funct. Mater.* **2010**, *20*, 3583-3594.
(31) Chen, S.; Hu, J.; Yuen, C.-W. M.; Chan, L.; Zhuo, H. Triple Shape Memory Effect in Multiple Crystalline Polyurethanes. *Polym. Advan. Technol.* **2010**, *21*, 377-380.
(32) Zhao, J.; Chen, M.; Wang, X.; Zhao, X.; Wang, Z.; Dang, Z.-M.; Ma, L.; Hu, G.-H.; Chen, F. Triple Shape Memory Effects of Cross-Linked Polyethylene/Polypropylene Blends with Cocontinuous Architecture. *ACS Appl. Mater. Interfaces* **2013**, *5*, 5550-5556.
(33) Niu, Y.; Zhang, P.; Zhang, J.; Xiao, L.; Yang, K.; Wang, Y. Poly(p-dioxanone)-Poly(ethylene glycol) Network: Synthesis, Characterization, and its Shape Memory Effect. *Polym. Chem.* **2012**, *3*, 2508-2516.
(34) Wang, L.; Yang, X.; Chen, H.; Yang, G.; Gong, T.; Li, W.; Zhou, S. Multi-Stimuli Sensitive Shape Memory Poly(vinyl alcohol)-Graft-Polyurethane. *Polym. Chem.* **2013,** *4*, 4461-4468.
(35) Xie, T. Tunable Polymer Multi-Shape Memory Effect. *Nature* **2010**, *464*, 267-270.
(36) Sun, L.; Huang, W. M. Mechanisms of the Multi-Shape Memory Effect and Temperature Memory Effect in Shape Memory Polymers. *Soft Matter* **2010**, *6*, 4403-4406.
(37) Han, Y.; Bai, T.; Liu, Y.; Zhai, X.; Liu, W. Zinc Ion Uniquely Induced Triple Shape Memory Effect of Dipole–Dipole Reinforced Ultra-High Strength Hydrogels. *Macromol. Rapid Comm.* **2012**, *33*, 225-231.
(38) Le, X.; Lu, W.; Zheng, J.; Tong, D.; Zhao, N.; Ma, C.; Xiao, H.; Zhang, J.; Huang, Y.; Chen, T. Stretchable Supramolecular Hydrogels with Triple Shape Memory Effect. *Chem. Sci.* **2016**, DOI: 10.1039/c6sc02354a.
(39) Xiao, Y.-Y.; Gong, X.-L.; Kang, Y.; Jiang, Z.-C.; Zhang, S.; Li, B.-J. Light-, pH- and Thermal-Responsive Hydrogels with the Triple-Shape Memory Effect. *Chem. Sci.* **2016**, *52*, 10609-10612.
(40) Balk, M.; Behl, M.; Nöchel, U.; Lendlein, A. Shape-Memory Hydrogels with Switching Segments Based on Oligo(ω-pentadecalactone). *Macromol. Mater. Eng.* **2012**, *297*, 1184-1192.

(41) Balk, M.; Behl, M.; Noechel, U.; Lendlein, A. Shape-Memory Hydrogels with Crystallizable Oligotetrahydrofuran Side Chains. *Macromol. Symp.* **2014**, *345*, 8-13.
(42) Pierce, B. F.; Bellin, K.; Behl, M.; Lendlein, A. Demonstrating the Influence of Water on Shape-Memory Polymer Networks Based on Poly[(rac-lactide)-co-glycolide] Segments in Vitro. *Int. J. Artif. Organs* **2011**, *34*, 172-179.
(43) Huang, W. M.; Yang, B.; An, L.; Li, C.; Chan, Y. S. Water-Driven Programmable Polyurethane Shape Memory Polymer: Demonstration and Mechanism. *Appl. Phys. Lett.* **2005**, *86*, 114105.
(44) Xing, Z.; Yang, G. Crystallization, Melting Behavior, and Wettability of Poly(ε-caprolactone) and Poly(ε-caprolactone)/ Poly(N-vinylpyrrolidone) Blends. *J. Appl. Polym. Sci.* **2010**, *115*, 2747-2755.
(45) Haaf, F.; Sanner, A.; Straub, F. Polymers of N-Vinylpyrrolidone: Synthesis, Characterization and Uses. *Polym. J.* **1985**, *17*, 143-152.
(46) Bittiger, H.; Marchessault, R. H.; Niegisch, W. D. Crystal Structure of Poly(epsilon -caprolactone). *Acta Crystallogr. Sect. B* **1970**, *26*, 1923-1927.
(47) Platé, N. A.; Shibaev, V. P. Comb-like Polymers. Structure and Properties. *J. Polym. Sci. Macromol. Rev.* **1974**, *8*, 117-253.
(48) Liu, L.-Z.; Chu, B. Crystalline Structure and Morphology of Microphases in Compatible Mixtures of Poly(tetrahydrofuran-methyl methacrylate) Diblock Copolymer and Polytetrahydrofuran. *J. Polym. Sci. B Polym. Phys.* **1999**, *37*, 779-792.
(49) Gazzano, M.; Malta, V.; Focarete, M. L.; Scandola, M.; Gross, R. A. Crystal Structure of Poly(omega-pentadecalactone). *J. Polym. Sci. Pol. Phys.* **2003**, *41*, 1009-1013.
(50) Scherrer, P. Bestimmung der Größe und der Inneren Struktur von Kolloidteilchen mittels Röntgenstrahlen. *Göttinger Nachrichten Math. Phys.* **1918**, *2*, 98-100.
(51) Wagermaier, W.; Zander, T.; Hofmann, D.; Kratz, K.; Narendra Kumar, U.; Lendlein, A. In Situ X-Ray Scattering Studies of Poly(ε-caprolactone) Networks with Grafted Poly(ethylene glycol) Chains to Investigate Structural Changes during Dual- and Triple-Shape Effect. *Macromol. Rapid Commun.* **2010**, *31*, 1546-1553.